Complex fission phenomena

D. N. Poenaru[1,2]*, R. A. Gherghescu*[1]*, and W. Greiner*[2]

[1]*Horia Hulubei National Instiute of Physics and Nuclear Engineering, PO Box MG-6, RO-077125 Bucharest-Magurele, Romania*

[2]*Frankfurt Institute for Advanced Studies, J W Goethe University, Pf. 111932, D-60054 Frankfurt am Main, Germany*

Abstract

Complex fission phenomena are studied in a unified way. Very general reflection asymmetrical equilibrium (saddle point) nuclear shapes are obtained by solving an integro-differential equation without being necessary to specify a certain parametrization. The mass asymmetry in binary cold fission of Th and U isotopes is explained as the result of adding a phenomenological shell correction to the liquid drop model deformation energy. Applications to binary, ternary, and quaternary fission are outlined.

PACS: 24.75.+i, 25.85.Ca, 27.90.+b, 23.70.+j

Keywords: NUCLEAR COLD FISSION, multicluster fission, true ternary fission, binary fission, saddle point shapes, integro-differential equation, mass asymmetry.

E-PRINT at http://arXiv.org: nucl-th/0404029.

1 Introduction

There is a continuous progress in deeper understanding the large variety of fission processes which can be theoretically treated in a unified way [1]. Even α-decay and cluster radioactivities [2, 3] can be considered among the members of this family. Particle accompanied fission was discovered in 1946 (see the review [4]), but only recently, by using new methods of fission fragment identification based on the characteristic rotational spectra measured with large arrays of Germanium Compton-suppressed detectors (as GAMMASPHERE) [5, 6], the "cold" processes α and ^{10}Be accompanied cold fission as well as the double and triple fine structure in a binary and ternary fission have been discovered [7]. The unified approach of cold binary fission, cluster radioactivity, and α-decay [1] was extended to cold ternary [8] and to multicluster fission including quaternary (two-particle accompanied) fission [9]. In that paper we stressed the expected enhanced yield of two alpha accompanied fission compared to other combinations of two light particles; it was indeed experimentally confirmed [10, 11]. In a cold binary fission the involved nuclei are neither excited nor strongly deformed, hence no neutron is evaporated from the fragments

or from the compound nucleus; the total kinetic energy equals the released energy. In a more complex than binary *cold fission* (ternary, quaternary, etc), neutrons could still be emitted from the neck, because the Q-value is positive. In this case their kinetic energy added to those of the fragments should exhaust the total released energy.

The importance of scission configuration for ternary fission [12] was repeatedly stressed in the past. In binary fission, it is now better understood due to a longstanding effort of systematic analysis [13, 14, 15, 16].

The statical approach was widely used [17, 18, 19] to find the saddle point shapes within a liquid drop model (LDM). Usually the equilibrium nuclear shapes are obtained by minimizing the energy functional on a certain class of trial functions representing the surface equation. Such an approach shows the importance of taking into account a large number of deformation coordinates (it seems that 5 coordinates are frequently needed) [20, 21]. The parametrization of Legendre polynomial expansion with even order deformation parameters α_{2n} up to $n = 18$ was employed [17] to describe various saddle point shapes including those very similar to two tangent spheres.

In order to study nuclear properties we have to consider both the collective and the single-particle motion of nucleons. This can be done by adding a shell correction to the LDM deformation energy [22]. Otherwise a well known asymmetrical mass distribution of fission fragments or the ground state deformation of the majority of nuclei could not be explained.

In this paper we present results obtained with a method allowing to find a general reflection symmetrical or asymmetrical saddle point shape as a solution of an integro-differential equation without a shape parametrization *apriori* introduced. This equation is derived as a Euler-Lagrange relationship associated to the variational problem of minimizing the potential energy with constraints (constant volume and given deformation parameter). The axially-symmetrical surface shape minimizing the liquid drop energy, $E_{LDM} = E_s + E_C$, is straightforwardly obtained. Minima of the saddle point deformation energy appear at finite values of the mass-asymmetry parameter as soon as the shell corrections, δE, are taken into account [23, 24]. A phenomenological shell correction is used. Also we shall discuss the multicluster fission phenomena.

2 Equilibrium shapes

In contrast to reality, within a liquid drop model all nuclear shapes in the ground-state are spherical and the fission fragment mass distributions are symmetrical. Permanent nuclear deformations and fission fragment mass asymmetry can be explained by combining the collective (liquid drop-like) and single particle properties in the framework of a macroscopic-microscopic method. By using the two center shell model to describe the single-particle states in binary fission or the three center shell model in the ternary fission, one can follow the shell structure all the way from the original nucleus, over the potential barriers, up to the final stage of separated fragments. Particularly important points on a potential energy surface are those corresponding to the ground-state, saddle point and scission point.

In order to illustrate the definition of the saddle point we plotted in figure 1 an example of a LDM potential energy surface (PES) versus two deformation parameters: the elongation R [or the dimensionless quantity $(R-R_i)/(R_t-R_i)$ where R_i and R_t are the initial and touching point values of the separation distance R] and the mass asymmetry $\eta = (A_1-A_2)/(A_1+A_2)$. A statical path may be seen on this PES as a heavy line following the valley of the potential minimum which corresponds to $\eta = 0$. If we start with a large value of R and then follow the decreasing elongations, the bottom of that valley leads to increasingly higher energies up to a maximum (the saddle point) marked with a cross on figure 1, then the energies along the valley are decreasing until the ground state minimum is reached. In this example the energy $E = E(R,\eta)$ is function of two shape coordinates and the fission valley represents a conditional minimum of the energy [$\partial E/\partial\eta = 0$ for different elongations $R = R_k$ $(k = 1, 2, ..., n)$ and $\eta = 0$]. The maximum value of this minimum is the saddle point defined by

$$\partial E/\partial\eta = \partial E/\partial R = 0 \tag{1}$$

$$\begin{vmatrix} \frac{\partial^2 E}{\partial R^2} & \frac{\partial^2 E}{\partial R \partial \eta} \\ \frac{\partial^2 E}{\partial \eta \partial R} & \frac{\partial^2 E}{\partial \eta^2} \end{vmatrix} < 0 \tag{2}$$

If we take another value of mass asymmetry $\eta = \eta_k \neq 0$, for every R_j within LDM, we obtain a new (conditional) saddle point at higher energy (see figure 2 where $d_L - d_R$ is proportional with η), proving that the mass asymmetric distribution of fission fragments is not explained by a pure LDM.

3 Integro-differential equation

We are looking for a function $\rho = \rho(z)$ expressing in cylindrical coordinates the nuclear surface equation with axial symmetry around z axis and the tips z_1 and z_2. The dependence on the neutron, N, and proton, Z, numbers is contained in the surface energy of a spherical nucleus, E_s^0, the fissility parameter $X = E_C^0/(2E_s^0)$, as well as in the shell correction of the spherical nucleus δE^0. E_C^0 is the Coulomb energy of the spherical shape for which the radius is $R_0 = r_0 A^{1/3}$ and the mass number $A = N + Z$. The radius constant is $r_0 = 1.2249$ fm, and $e^2 = 1.44$ MeV·fm is the square of electron charge. The lengths are given in units of the radius, R_0, and the Coulomb potential at the nuclear surface, $V_s = (R_0/Ze)\phi_s$, in units of Ze/R_0. The surface tension and the charge density are denoted by σ and ρ_e respectively. The nuclear surface equation we are looking for should minimize the functional of potential energy of deformation

$$E_s + E_C = 2\pi\sigma R_0^2 \int_{z_1}^{z_2} \rho(z)\sqrt{1+\rho'^2}dz + \frac{2\pi R_0^2 Ze\rho_e}{5}\int_{z_1}^{z_2}\left(\rho^2 - \frac{z}{2}\frac{\partial\rho^2}{\partial z}\right)V_s dz \tag{3}$$

with two constraints: volume conservation,

$$V = \pi R_0^3 \int_{z_1}^{z_2} \rho^2(z)dz = \frac{4\pi R_0^3}{3} \tag{4}$$

and a given deformation parameter,

$$\alpha = \frac{\pi R_0^3}{V} \int_{z_1}^{z_2} F(z,\rho)\rho^2 dz \tag{5}$$

assumed to be an adiabatic variable.

According to the calculus of variations [25] the function $\rho(z)$ minimizing the energy with two constraints should satisfy the Euler-Lagrange equation (see the Appendix)

$$\rho\rho'' - \rho'^2 - (\lambda_1 + \lambda_2|z| + 6XV_s)\,\rho(1+\rho'^2)^{3/2} - 1 = 0 \tag{6}$$

or

$$2\sigma K + 3\rho_e\phi_s/5 + \lambda_1' + \lambda_2'|z| = 0 \tag{7}$$

where λ_1' and λ_2' are Lagrange multipliers and K is the mean curvature [26]:

$$K = (\mathcal{R}_1^{-1} + \mathcal{R}_2^{-1})/2 \tag{8}$$

with $\mathcal{R}_1$ and $\mathcal{R}_2$ the principal radii of curvature given by

$$\mathcal{R}_1 = R_0\tau\rho \;\;;\;\; \mathcal{R}_2 = -R_0\tau^3/\rho'' \;\;;\;\; \tau^2 = 1+\rho'^2 \tag{9}$$

where $\rho' = d\rho/dz$ and $\rho'' = d^2\rho/dz^2$.

It is interesting to mention that in the absence of an electric charge, the condition of stable equilibrium at the surface of a fluid [27, 28] is given by Laplace formula equating the difference of pressures with the product $2\sigma K$.

By choosing the deformation coordinate as the distance between the centers of mass of the left and right fragments, $\alpha = |z_L^c| + |z_R^c|$, one can reach all intermediate stages of deformation from one parent nucleus to two fragments by a continuos variation of its value. Also a possible dynamical study, for which the center of mass treatment is very important [29], may conveniently use this definition of the deformation parameter. The position of separation plane between fragments, $z = 0$, is given by the condition $(d\rho/dz)_{z=0} = 0$, which defines the median plane for a usual spherical, ellipsoidal, or "diamond" shape in the ground state, or the middle of the neck for an elongated reflection symmetrical shape on the fission path. For this choice of the function $F(z,\rho)$ one has $f = |z|$.

At the left hand side and right hand side tips on the symmetry axis one can write

$$\rho(z_1) = \rho(z_2) = 0 \tag{10}$$

and the transversality conditions

$$\frac{d\rho(z_1)}{dz} = \infty \;\;;\;\; \frac{d\rho(z_2)}{dz} = -\infty \tag{11}$$

The equation is solved numerically by an iterative procedure checking the minimization of the deformation energy with a given accuracy. The phenomenological shell corrections to the LDM deformation energy presented in section 5 are used to obtain reflection asymmetric saddle point shapes. In fact the equation to be solved numerically is obtained from (6) after changing the variable and function as shown below.

One can develop the computer code for just one of the "fragments" (for example for the right hand one extended from $z = 0$ to $z = z_2$) and then write the result for the other fragment (left hand one from $z = -z_1$ to $z = 0$). For symmetrical shapes we have $z_2 = z_p = -z_1$. It is convenient to make a change of the function and variable defined by:

$$u(v) = \Lambda^2 \rho^2[z(v)] \;\; ; \;\; z(v) = z_p - v/\Lambda \tag{12}$$

therefore $dz/dv = -1/\Lambda$, $u' = du/dv = 2\Lambda^2 \rho (d\rho/dz) dz/dv = -2\Lambda\rho\rho'$, $\rho = \sqrt{u}/\Lambda$, $u'^2 = 4u\rho'^2$, $1 + \rho'^2 = u'^2/(4u) + 1$, $u'' = d^2u/dv^2 = d(u')/dv = -2\Lambda[d\rho(z(v))/dv]d\rho/dz - 2\Lambda\rho d(\rho(z(v))/dz = -2\Lambda(d\rho/dz)(dz/dv)(d\rho/dz) - 2\Lambda\rho(d^2\rho/dz^2)dz/dv = 2\rho'^2 + 2\rho\rho''$. By substituting into equation (6) one has

$$u'' - 2 - \frac{1}{u}\left[u'^2 + \left(\frac{3XV_s}{2\Lambda} + \frac{\lambda_1 + \lambda_2 z_p}{4\Lambda} - \frac{\lambda_2 v}{4\Lambda^2}\right)(4u + u'^2)^{3/2}\right] = 0 \tag{13}$$

A linear function of v is introduced by adding and subtracting $a + bv$ to $3XV_s/2\Lambda$. The quantity V_{sd} is defined as the deviation of Coulomb potential at the nuclear surface from a linear function of v

$$V_{sd} = \frac{3X}{2\Lambda} V_s - a - vb \tag{14}$$

where the constant

$$a = \frac{3X}{2\Lambda} V_s(v = 0) \tag{15}$$

is chosen to give $V_{sd}(v = 0) = 0$, and

$$b = \left[\frac{3X}{2\Lambda} V_s(v = v_p) - a\right] / v_p \tag{16}$$

where $v_p = \Lambda z_p$. Consequently one has

$$u'' - 2 - \frac{1}{u}\left\{u'^2 + \left[\left(\frac{\lambda_1 + \lambda_2 z_p}{4\Lambda} + a\right) + v\left(b - \frac{\lambda_2}{4\Lambda^2}\right) + V_{sd}\right](4u + u'^2)^{3/2}\right\} = 0 \tag{17}$$

By equating with 1 the coefficient of v, one can establish the following link between Λ and the Lagrange multiplier λ_2

$$\Lambda^2 = \lambda_2/4(b - 1) \tag{18}$$

In this way $u(v)$ is to be determined by the equation

$$u'' - 2 - \frac{1}{u}[u'^2 + (v - d + V_{sd})(4u + u'^2)^{3/2}] = 0 \tag{19}$$

where the role of a Lagrange multiplier is played by the quantity d which is taken to be constant instead of α. The value of the deformation coordinate α is calculated after obtaining a convergent solution. To the tip $z = z_p$, at which $\rho(z_p) = 0$, corresponds $v = 0$, hence $u(0) = \Lambda^2 \rho^2(z_p) = 0$. By multiplying with u the equation (19), introducing $v = 0$, and using the relationship $V_{sd}(v = 0) = 0$, it follows that $u'(0) = 1/d$. Consequently the boundary conditions for $u(v)$ are:

$$u(0) = 0, \;\; u'(0) = 1/d \tag{20}$$

To $z = 0$, at which $\rho'(0) = 0$ (the middle of the neck for elongated shapes), corresponds $v_p = \Lambda z_p$ and $u'(v_p) = -2\Lambda\rho(0)\rho'(0) = 0$. The point $v = v_p$ in which

$$u'(v_{pn}) = 0 \tag{21}$$

is determined by interpolation from two consecutive values of v_p leading to opposite signs of $u'(v)$. The number n of changes of signs is equal to the number of necks plus one given in advance, e.g. for a single neck (binary fission) $n = 2$ and for two necks (ternary fission) $n = 3$, etc.

Although the quantity Λ is not present in eq (19) we have to know it in order to obtain the shape function $u(v)$. By changing the function and the variable in the eq (4) one has

$$\Lambda = \left\{ \frac{3}{2} \int_0^{v_{pn}} u(v) dv \right\}^{1/3} \tag{22}$$

and the deformation coordinate, $\alpha = z_L^c + z_R^c$, may also be determined by adding to

$$z_R^c = 2\pi R_0^3 \int_0^{z_p} z\rho^2(z) dz/V = \frac{3}{2} \int_{v_p}^0 \frac{v_p - v}{\Lambda} \frac{u}{\Lambda^2} \frac{-dv}{\Lambda} = \frac{3}{2\Lambda^4} \int_0^{v_p} (v_p - v) u(v) dv \tag{23}$$

a similar relationship for z_L^c. From the dependence $\alpha(d)$, one can obtain the inverse function $d = d(\alpha)$.

In order to find the shape function $u(v)$ we solve eq (19) with boundary conditions written above. One starts with given values of the constants d and n. For reflection symmetric shapes $d_L = d_R$ and $n_L = n_R$. In the first iteration one obtains the solution for a Coulomb potential at the nuclear surface assumed to be a linear function of v, i.e. for $V_s = 0$. Then one calculates the parameters Λ, a, and b, which depend on the Coulomb potential and its deviation V_{sd} from a linear function, and the deformation energy corresponding to the nuclear shape [30, 31]. The quantity V_{sd} determined in such a way is introduced in eq (19) and the whole procedure is repeated until the deformation energy is obtained with the desired accuracy. In every iteration the equation is solved numerically with the Runge-Kutta method.

One can calculate for different values of deformation α (in fact for a given d_L and d_R) the deformation energy $E_{def}(\alpha)$. The particular value α_s for which $dE_{def}(\alpha_s)/d\alpha = 0$ corresponds to the extremum, i.e. the shape function describes the saddle point, and the unconditional extremum of the energy is the fission barrier. The other surfaces (for $\alpha \neq \alpha_s$) are extrema only with condition $\alpha =$ constant. In this way one can compute the deformation energy versus $d_L = d_R$. In Fig. 3 one can see an example of variation of deformation parameter and the deformation energy with d_L for ^{238}U at symmetry $\eta = 0$. The saddle point corresponds to the maximum of deformation energy.

For *reflection asymmetrical shapes* we need to introduce another constraint: the asymmetry parameter, η, defined by

$$\eta = \frac{M_L - M_R}{M_L + M_R} = \frac{A_1 - A_2}{A_1 + A_2} \tag{24}$$

It should remain constant during variation of the shape function $u(v)$. Consequently eq (19) should be written differently for left hand side and right hand side. Now d_L is

different from d_R, and so are the parameters Λ_L and Λ_R. They have to fulfil matching conditions

$$\rho_L(z=0) = \rho_R(z=0) \tag{25}$$

hence

$$u_L^{1/2}(v_p)/\Lambda_L = u_R^{1/2}(v_p)/\Lambda_R \tag{26}$$

The similar condition for derivatives $\rho'(z)$ in $z=0$,

$$\rho'_L(z=0) = \rho'_R(z=0) = 0 \tag{27}$$

is automatically satisfied due to eq (21). The second derivative $\rho''(z)$ can have a discontinuity in $z=0$ if $d_L \neq d_R$. The parameters Λ_L and Λ_R are easily expressed in terms of η, if we write the definition of mass asymmetry as

$$M_L = \frac{2\pi}{3}(1+\eta) = \pi\Lambda_L^{-3}\int_0^{v_p} u_L(v)dv \tag{28}$$

$$M_R = \frac{2\pi}{3}(1-\eta) = \pi\Lambda_R^{-3}\int_0^{v_p} u_R(v)dv \tag{29}$$

We assume that $M_L + M_R$ is equal to the mass of a sphere with $R_0 = 1$. It follows

$$\Lambda_L = (1+\eta)^{-1/3}\Lambda_{L0} \tag{30}$$

$$\Lambda_R = (1-\eta)^{-1/3}\Lambda_{R0} \tag{31}$$

where we introduced notations similar to eq (22):

$$\Lambda_{L0(R0)} = \left\{\frac{3}{2}\int_0^{v_p} u_{L(R)}(v)dv\right\}^{1/3} \tag{32}$$

The shape of a nucleus with given mass asymmetry, η, is completely determined by the above written equations in which the quantities $u_L(v_p)$ and $u_R(v_p)$ are solutions of the eq (19). There is an almost linear dependence of η from the difference $d_L - d_R$.

4 Mass symmetry in binary fission within LDM

One can test the method by comparing some nuclear shapes within LDM to the standard results for medium and heavy nuclei. In Figure 4 we present reflection symmetric nuclear shapes for binary fission of a nucleus with the fissility parameter $X = 0.6$ (e.g. ^{170}Yb), obtained for $n_L = n_R = 2$ (one neck), $d_L = d_R = 1.4; 1.5; 1.7$, and 1.91 (for which $\alpha = 1.314; 1.644; 2.100$ and 2.304) and a vanishing mass asymmetry $\eta = 0$. The saddle point (maximum value of the conditioned deformation energy minimum) is obtained for $d_L = 1.91$, at which the shape is deformed and necked-in.

A comparison between three nuclear shapes at the saddle point for nuclei with fissilities $X = 0.60, 0.70$, and 0.82 (corresponding to ^{170}Yb, ^{204}Pb, and ^{252}Cf nuclei lying on the line of beta-stability) is presented in Figure 5. One can see how the necking-in and the elongation are decreasing ($\alpha = 2.304; 1.822$ and 1.165) when fissility increases from $X = 0.60$ to $X = 0.82$, in agreement with [17]. In the limit $X = 1$ the saddle point shape is spherical. The method proved its capability by reproducing the well known LDM saddle point shapes.

5 Mass asymmetry in binary fission

Within LDM a nonzero mass asymmetry parameter (see the shapes from figure 6) leads to a deformation energy which increases with η as is illustrated in figure 2, where η is replaced by an almost linear dependent quantity $(d_L - d_R)$. The reflection asymmetric shapes plotted in figure 6, resulted by choosing the input parameters as follows: $n_L = n_R = 2$; $d_L = 1.40; 1.45; 1.50$, and 1.60 while $d_R = 1.40$ was kept constant, and so was $X = 0.60$. The increasing deformation energy with mass-asymmetry in figure 2, refers to different values of fissility, namely $X = 0.758$ for ^{228}Th.

When the shell effects are taken into account a saddle point solution of the integro-differential equation with reflection asymmetry is obtained. In the following we shall use a phenomenological shell correction adapted after Myers and Swiatecki [32]. At a given deformation one calculates the volumes of fragments and the corresponding numbers of nucleons $Z_i(\alpha),\ N_i(\alpha)$ $(i = 1, 2)$, proportional to the volume of each fragment. Then one can add for each fragment the contribution of protons and neutrons

$$\delta E(\alpha) = \sum_i \delta E_i(\alpha) = \sum_i [\delta E_{pi}(\alpha) + \delta E_{ni}(\alpha)] \tag{33}$$

given by

$$\delta E_{pi} = Cs(Z_i); \quad \delta E_{ni} = Cs(N_i) \tag{34}$$

where

$$s(Z) = Z^{-2/3} F(Z) - cZ^{1/3} \tag{35}$$

and similar eq for $s(N)$.

$$F(n) = \frac{3}{5}\left[\frac{N_i^{5/3} - N_{i-1}^{5/3}}{N_i - N_{i-1}}(n - N_{i-1}) - n^{5/3} + N_{i-1}^{5/3}\right] \tag{36}$$

where $n \in (N_{i-1}, N_i)$ is the current number of protons (Z) or neutrons (N) and N_{i-1}, N_i are the nearest magic numbers. The parameters $c = 0.2$, $C = 6.2$ MeV were determined by fit to experimental masses and deformations.

The dependence on deformation [33] α is given by

$$\delta E(\alpha) = \frac{C}{2}\left\{\sum_i [s(N_i) + s(Z_i)]\frac{L_i(\alpha)}{R_i}\right\} \tag{37}$$

where $L_i(\alpha)$ are the lenghths of fragments along the symmetry axis. During the deformation process, the variation of separation distance between centers, α, induces the variation of the geometrical quantities and of the corresponding nucleon numbers. Each time a proton or neutron number reaches a magic value, the correction energy passes through a minimum, and it has a maximum at midshell.

Results for binary cold fission of parent nuclei $^{226-238}$Th and $^{230-238}$U are presented in figures 8 and 9. The minima of the saddle point energy occur at nonzero mass asymmetry parameters $d_L - d_R$ in the range $0.04, 0.08$ for the above mentioned nuclei. They correspond to η of $0.050, 0.095$ which leads to $A_1 \simeq 125$ in all cases. A typical saddle point shape, for

^{232}U may be seen in figure 7. For experimentally determined mass asymmetry [34, 35] the maximum of the fission fragment mass distributions is centered on $A_1 = 140$ in a broad range of mass numbers of parent nuclei.

In order to understand correctly the figure 8, where from the saddle point energies E_{SP} of every nucleus we subtracted its minimum value E_{SP}^{min}, we would like to give an example for ^{238}U in figure 10. In the upper part we plot the saddle point energies obtained within a pure LDM (see also Fig. 2). When we add the shell corrections, the conditions of equilibrium are changed and in general the LDM part of the saddle point energy is not identical with the previous one, as may be also seen from the tables 1 and 2. Table 2 shows how are changed equilibrium conditions when the shell effects are taken into account. There are two rows for every value of $d_L - d_R$ when $d_L - d_R < 0.045$: one for maximum value of the total E_{SP}, and the other one for maximum value of its LDM term E_{SP-LDM}.

The minimum of the E_{SP} is produced by the negative values of the shell corrections $\delta E - \delta E^0$ which can be clearly seen in the lower part of the figure 10. The variation of the saddle point energy with the mass asymmetry parameter $d_L - d_R$ is almost a linear function of the mass asymmetry η for some even-mass isotopes of Th and U. The minima of the saddle point energy occur at nonzero mass asymmetry parameters $d_L - d_R$ between about 0.04 and 0.085 for these nuclei. When the mass number of an isotope increases, the value of the mass asymmetry corresponding to the minimum of the SP energy decreases.

As mentioned by Wilkins et al. [36], calculations of PES for fissioning nuclei "qualitatively account for an asymmetric division of mass". From the qualitative point of view the results displayed in Figures 8 and 9 proove the capability of the method to deal with fission mass and charge asymmetry. The experimentally determined mass number of the most probable heavy fragment [37] for U isotopes ranges from 134 to 140. The corresponding values at the displayed minima in Figures 8 and 9 are very close to 125, which means a discrepancy between 6.7 % and 10.7 % for A_H. The inaccuracy in reproducing the experimental mass asymmetry is due to the contribution of the phenomenological shell corrections. In the absence of shell corrections the pure liquid drop model (LDM) reflection-symmetric saddle point shapes [17] are reproduced, and the barrier height increseas with an increased mass asymmetry. When the shell corrections are taken into account the LDM part behaves in the same manner (larger values at non-zero mass asymmetry). Only the contribution of shell effects can produce a minimum of the barrier height at a finite value of the mass asymmetry. One may hope to obtain a better agreement with experimental data by using a more realistic shell correction model, based for example on the recently developed two center shell model [38].

6 Ternary Fission

Neutron multiplicities higher than one, in the induced nuclear fission, are used to produce the chain reaction, on which the nuclear energetics is based. The condition of a positive released energy, $Q > 0$, in such a complex process is easily fulfilled, and the escape of one or several neutrons from the neck formed between the light- and heavy fragment, is not prevented by any Coulomb barrier. A small and narrow centrifugal barrier, due to

the angular momenta carried away by the neutrons, do not constitute a major obstacle. A charged particle has to penetrate, by quantum tunneling, a much thicker and higher potential barrier, leading to a long delay and to a corresponding comparable low yield. Nevertheless, the particle-accompanied fission (or ternary fission) was observed both in neutron-induced and spontaneous fission since 1946. Several such processes, in which the charged particle is a proton, deuteron, triton, $^{3-8}$He, $^{6-11}$Li, $^{7-14}$Be, $^{10-17}$B, $^{13-2}$C, $^{15-20}$N, $^{15-22}$O, have been detected [4]. Many other heavier isotopes of F, Ne, Na, Mg, Al, Si, P, S, Cl, Ar, and even Ca were also mentioned.

Different elongated shapes for ternary fissions are shown in figure 11. For shapes with three fragments and two necks ($n_L = n_R = 3$) when $d_L = d_R$ is increased from 2.25 to 2.80 and 7.00 the deformation α increases from 1.650 to 2.306 and 2.730. In the same time the elongation is initially increased from 5.234 to 5.392 and then decreased to 5.24; the fragment radii are 0.461/0.814/0.461, 0.592/0.753/0.592, and 0.673/0.659/0.673, leading to decreasing energies in units of E_s^0 from 0.165 to 0.150 and 0.134. The configuration with $E/E_s^0 = 0.134$ is not far from a *"true ternary-fission"* in which the three fragments are almost identical: $^{170}_{70}$Yb$\rightarrow^{56}_{23}$V + $^{56}_{23}$V + $^{58}_{24}$Cr and the Q-value is 83.639 MeV. One may compare the above E/E_s^0 value with the touching-point energy of these spherical fragments $(E_t - Q)/E_s^0 = 0.239$. It is larger, as expected, because of the finite neck of the shapes in figure 11. For α-accompanied fission of ^{170}Yb with two $^{83}_{34}$Se fragments $Q = 87.484$ MeV is larger and the touching point energy $(E_t - Q)/E_s^0 = 0.103$ is lower. A lower $Q = 70.859$ MeV and higher energy barrier $(E_t - Q)/E_s^0 = 0.147$ is obtained for ^{10}Be accompanied fission of ^{170}Yb with $^{80}_{33}$As fission fragments.

Figure 12 shows how evolves the ternary shapes for three values of the fissility ($X = 0.60$ corresponding to ^{170}Yb, $X = 0.7716$ corresponding to ^{236}U and $X = 0.8213$ e.g. ^{252}Cf) when the input paramter $d_L = d_R$ is increased. For smaller values of $d_L = d_R$ the elongation of the shapes becomes larger up to a limiting value of about 3, 4 and 4.3 respectively; then if $d_L = d_R$ is further increased it becomes slightly smaller. In what concerns the shapes approaching the scission into three identical fragments (figure 13) the total length increases with increasing fissility.

Systematic calculations [39] have shown a clear correlation between the Q-values and the measured yield of different isotopes for one cluster accompanied fission. For example, among the He isotopes with mass numbers 4, 6, and 8, ^{4}He leads to the maximum Q-value. The maximum yield was indeed experimentally observed [4] for α accompanied fission. Similarly, among ^{6,8,10,12}Be, the clusters ^{8}Be and ^{10}Be give the maximum Q-values. As ^{8}Be spontaneously breaks into 2α particles it is not easy to measure ^{8}Be accompanied fission yield; consequently ^{10}Be has been most frequently identified. *By detecting, in coincidence, these two alpha particles, the ^{8}Be accompanied fission with a larger yield compared to that of the ^{10}Be one, could be observed in the future.* From ^{12,14,16,18}C the favoured is ^{14}C, and all ^{16,18,20,22}O isotopes have comparable Q-values when they are emitted in a cold binary fission of ^{252}Cf. Nevertheless, ^{20}O is slightly upper than the others. As a rule, if the Q-value is larger the barrier height is smaller, and the quantum tunneling becomes more probable. The stronger emission of ^{14}C compared to ^{12}C has the same explanation as for the ^{14}C radioactivity; the Q-value is larger because the heavy fragment is doubly magic.

We should stress again that if one is interested to estimate the yield in various fission processes, one has to compare the potential barriers and not the Q-values. Our results

are in agreement with preceding calculations [40] showing also preference for prolate over oblate shapes. Theoretically it was pointed out by Present [41] in 1941 that Uranium tripartition would release about 20 MeV more energy than the binary one. In spite of having quite large Q values [39], this "true ternary fission" is a rather weak process; the strongest phenomenon remains the α-particle-accompanied fission.

Experiments on so-called "symmetrical tripartition" were performed *e.g.* using the induced fission of ^{235}U by thermal neutrons [42], the induced fission of ^{238}U by intermediate-energy hellium ions [43], or spontaneous fission of ^{252}Cf [44], etc. An yield of 6.7 ± 3.0 per 10^6 binary fissions was reported by Rosen and Hudson [42] who employed a triple gas-filled ionization chamber and a suitable electronics including a triple coincidence circuit. Other "optimistic" results are mentioned by Iyer and Cobble [43], who tried radiochemical methods of identification at intermediate energy of excitation. While at high energy [45] implying bombarding heavy ions of several hundred MeV, a positive result may be accepted, it is not certain whether it comes out from a compund nucleus. The general conclusion [44] after measuring triple coincidences with detectors placed at 120° is rather pessimistic: except for excitation energies over 24 MeV, the true ternary yield is extremely low: under 10^{-8} per binary fission act. By performing dynamical calculations, Hill arrived in his thesis and in [46] at elongated shapes with pronounced necks looking more encouraging for particle-accompanied fission. It would be rewarding to perform successful experiments with nowadays very much improved experimental techniques, despite the previous rather pessimistic conclusion that "true" ternary spontaneous fission is an extremely rare phenomenon.

7 Multicluster fission

The shapes with four fragments and three necks ($n_L = n_R = 4$) can be seen in figure 15. When $d_L = d_R$ increases from 2.30 to 2.70 and 4.00 the deformation takes the values 2.144, 3.136, and 3.233 and the elongations are 6.077, 6.916 and 6.252. The fragment radii are 0.408/0.625/0.625/0.408, 0.479/0.632/0.632/0.479, and 0.608/0.616/0.616/0.608, for which the energies in units of E_s^0 are 0.188, 0.216 and 0.214, respectively. The last shape, with $E/E_s^0 = 0.214$ approaches a fission into almost identical four fragments $^{170}_{70}$Yb$\rightarrow^{42}_{17}$Cl + $^{42}_{17}$Cl + $^{43}_{18}$Ar + $^{43}_{18}$Ar. Again the configuration with aligned spherical fragments in touch is higher in energy: $(E_t - Q)/E_s^0 = 0.324$. Even more complex shapes can be obtained by further increasing the values of $n_L = n_R$.

In 1958 it was theoretically shown [47] on the basis of the liquid drop model [32] that for increasingly heavier nuclei, fission into three, then four and even five fragments becomes energetically more favourable than binary fission (see figure 14). One can take, as an approximation of the Q value, the energy difference between the sum of Coulomb and surface energies for the parent (superscript ^{0}) and n identical fission fragments (superscript ^{i})

$$Q_n \simeq (E_C^0 + E_s^0) - \sum_{i=1}^{n} (E_C^i + E_s^i) \tag{38}$$

where $n = 2$ for binary fission, $n = 3$ for ternary fission, $n = 4$ — a quaternary fission, $n = 5$ — a division into five fragments, $n = 6$ — a division into six fragments, etc.

A linear dependence of Q_n on the (binary) fissility parameter, $X = E_C^0/(2E_s^0)$, of the form

$$Q_n/E_s^0 \simeq 1 - n^{1/3} + 2X(1 - n^{-2/3}) \tag{39}$$

has been obtained [47]. When the fissility parameter increases, fission into more than two equal fragments becomes energetically favored. At $X \geq 0.426$ tripartition becomes exothermic and for $X \geq 0.611$ the Q-value for fission into three identical fragments is larger than that for binary fission. The general trend, and sometimes even the absolute values of Q_2 and Q_3, are well reproduced [39] by the above equation.

A better chance to be experimentally observed has a quaternary fission in which two light particles are emitted from a neck formed between two heavy fragments [9, 50]. The successful experiment [10, 11] on 2α-accompanied fission observed in cold neutron induced fission of ^{233,235}U, confirmed our expectations.

The possibility of a whole family of new decay modes, *the multicluster accompanied fission*, was envisaged [48, 9, 49, 50]. Besides the fission into two or three fragments, a heavy or superheavy nucleus spontaneously breaks into four, five or six nuclei of which two are asymmetric or symmetric heavy fragments and the others are light clusters, e.g. α-particles, ^{10}Be, ^{14}C, ^{20}O, or combinations of them. Examples were presented for the two-, three- and four cluster accompanied cold fission of ^{252}Cf and ^{262}Rf, in which the emitted clusters are: 2α, α+^{6}He, α+^{10}Be, α+^{14}C, 3α, α+^{6}He + ^{10}Be, 2α+^{6}He, 2α+^{8}Be, 2α+^{14}C, and 4α. A comparison was made with the recently observed ^{252}Cf cold binary fission, and cold ternary (accompanied by α particle or by ^{10}Be cluster). The strong shell effect corresponding to the doubly magic heavy fragment ^{132}Sn is emphasized. From the analysis of different configurations of fragments in touch, we conclude that the most favorable mechanism of such a decay mode should be the cluster emission from an elongated neck formed between the two heavy fragments.

In a first approximation, one can obtain an order of magnitude of the potential barrier height by assuming spherical shapes of all the participant nuclei. This assumption is realistic if the fragments are magic nuclei. For deformed fragments it leads to an overestimation of the barrier. By taking into account the prolate deformations, one can get smaller potential barrier height, hence better condition for multicluster emission. We use the Yukawa-plus-exponential (Y+E) double folded model [51, 52] extended [31] for different charge densities. In the decay process from one parent to several fragments, the nucleus deforms, reaches the touching configuration, and finally the fragments became completely separated.

Within the Myers-Swiatecki's liquid drop model there is no contribution of the surface energy to the interaction of the separated fragments; the deformation energy has a maximum at the touching point configuration. The proximity forces acting at small separation distances (within the range of strong interactions) give rise in the Y+EM to a term expressed as folllows

$$E_{Yij} = -4\left(\frac{a}{r_0}\right)^2 \sqrt{a_{2i}a_{2j}}\left[g_i g_j\left(4 + \frac{R_{ij}}{a}\right) - g_j f_i - g_i f_j\right]\frac{\exp(-R_{ij}/a)}{R_{ij}/a} \tag{40}$$

where

$$g_k = \frac{R_k}{a}\cosh\left(\frac{R_k}{a}\right) - \sinh\left(\frac{R_k}{a}\right)\ ;\ f_k = \left(\frac{R_k}{a}\right)^2 \sinh\left(\frac{R_k}{a}\right) \tag{41}$$

in which R_k is the radius of the nucleus A_kZ_k, $a = 0.68$ is the diffusivity parameter, and a_{2i}, a_{2j} are expressed in terms of the model constants a_s, κ and the nuclear composition parameters I_i and I_j, $a_2 = a_s(1 - \kappa I^2)$, $a_s = 21.13$ MeV, $\kappa = 2.3$, $I = (N - Z)/A$, $R_0 = r_0 A^{1/3}$, $r_0 = 1.16$ fm is the radius constant, and e is the electron charge, $e^2 \simeq 1.44$ MeV·fm.

In order to emphasize the strong shell effect, we have chosen in the abscisa of the figure 16 the number of neutrons of the light fragment, N_L, which in turn corresponds to a well defined neutron number of the heavy fragment, N_H, for a given parent and a given cluster accompanied fission, in our case to: $N_H = 150 - N_L$ for 2α accompanied fission, $N_H = 148 - N_L$ for 3α accompanied fission, and $N_H = 146 - N_L$ for 4α accompanied fission of ^{252}Cf. The vertical heavy bar on each plot helps to determine the position of the magic number $N_H = 82$. In a similar way, different types of lines are drawn through the points belonging to the same combination of atomic numbers of the fragments $Z_L - Z_H$. The red full line is always reserved for the pair in which the heavy fragment is an isotope of Sn, (with $Z_H = 50$ magic number). The conclusion is clear: the maximum Q-value is obtained when the heavy fragment is the doubly magic ^{132}Sn.

In figure 16 the investigated pairs are emphasized. These are [5] for the binary fission: $^{102,104}_{40}$Zr–$^{150,148}_{58}$Ce ($N_L = 62, 64$), $^{104-108}_{42}$Mo–$^{148-144}_{56}$Ba ($N_L = 62 - 66$), $^{110}_{44}$Ru–$^{142}_{54}$Xe ($N_L = 66$), and $^{116}_{46}$Pd–$^{136}_{52}$Te ($N_L = 70$). For cold α accompanied fission [7] one has: $^{92}_{36}$Kr–$^{156}_{60}$Nd ($N_L = 56$), $^{96-101}_{38}$Sr–$^{152-147}_{58}$Ce ($N_L = 58 - 63$), $^{100-104}_{40}$Zr–$^{148-144}_{56}$Ba ($N_L = 60 - 64$), $^{106-108}_{42}$Mo–$^{142-140}_{54}$Xe ($N_L = 64 - 66$), $^{112}_{44}$Ru–$^{136}_{52}$Te ($N_L = 68$), and $^{116}_{46}$Pd–$^{132}_{50}$Sn ($N_L = 70$). There is also one example of detected cold ^{10}Be accompanied fission of ^{252}Cf, namely $^{96}_{38}$Sr–$^{146}_{56}$Ba ($N_L = 58$).

On the right hand side of this figure there are plots for the new decay modes which have a good chance to be detected: 2α-, 3α-, and 4α accompanied fission. The corresponding Q-values are not smaller compared to what has been already measured, which looks very promising for the possibilty of detecting the 2α-, 3α-, and 4α accompanied fission decay modes. In fact by taking into account the mass-values of the participants, one can see that the Q-value for the 2α accompanied fission may be obtained by translation with +0.091 MeV from the Q-value of the ^{8}Be accompanied fission. A similar translation with -7.275 MeV should be made from the ^{12}C accompanied fission in order to obtain the Q-values of the 3α accompanied fission, etc. Less promising looks the combination of three cluster, α+^{6}He + ^{10}Be accompanied cold fission of ^{252}Cf. As mentioned above, the 2α accompanied fission was already observed.

Different kinds of aligned and compact configurations of fragments in touch are shown in figure 17. On the left hand side there are three aligned fragments on the same axis, in the following order of the three partners: 213, 123, and 132 (or 231) and one compact configuration (in which every partner is in touch with all others). It is clear that the potential barrier for the "polar emission" (123 or 132) is much higher than that of the emission from the neck (213), which explains the experimentally determined low yield of the polar emission compared to the "equatorial" one. As it should be, the compact configuration posses the maximum total interaction energy, hence it has the lowest chance to be observed. The same is true for the quaternary fission when the two clusters are formed in the neck (middle part of the figure). An important conclusion can be drawn, by generalizing this result, namely: *the multiple clusters* $1, 2, 3, \ldots$ *should be formed in*

a configuration of the nuclear system in which there is a relatively long neck between the light ($n-1$) and heavy (n) fragment. Such shapes with long necks in fission have been considered [46] as early as 1958. For the "true" ternary fission, in two ^{84}As plus ^{84}Ge, $E_t = 98$ MeV! Despite the larger Q-value (266 MeV), the very large barrier height explains why this split has a low chance to be observed.

On the right-hand side of figure 17, we ignore the aligned configurations in which the heavy fragments are not lying at the two ends of the chain. By arranging in six different manners the α-particle, ^{6}He, and ^{10}Be clusters between the two heavy fragments from the cold fission of ^{252}Cf, the difference in energy is relatively small. Nevertheless, the 43125 configuration seems to give the lowest barrier height.

The energies of the optimum configuration of fragments in touch, for the 2α-, 3α-, and 4α accompanied cold fission of ^{252}Cf are not much higher than what has been already measured. When the parent nucleus is heavier, the multicluster emission is stronger as we observed by performing calculations for nuclei like ^{252,254}Es, ^{255,256}Fm, ^{258,260}Md, ^{254,256}No, ^{262}Lr, ^{261,262}Rf, etc.

While the minimum energy of the most favorable aligned configuration of fragments in touch, when at least one cluster is not an alpha particle, becomes higher and higher with increasing complexity of the partners, the same quantity for multi alphas remains favorable. In conclusion, we suggested since 1998 experimental searches for the multicluster 2α accompanied fission, for ^{8}Be-, ^{14}C- and ^{20}O accompanied fission. Also, the contribution of the single- and multi-neutron accompanied cold fission mechanism to the prompt neutron emission has to be determined.

8 Conclusions

The method of finding the most general axially-symmetric shape at the saddle point without introducing *apriori* a parametrization (inherently limited due to the finite number of deformation coordinates), by solving an integro-differential equation was tested for binary, ternary, and quaternary fission processes within a pure liquid drop model. The well known LDM saddle point shapes are well reproduced. The method proved its practical capability in what concerns fission into two, three, or four identical fragments, for which fission barriers given by shapes with rounded necks are, as expected, lower than those of aligned spherical fragments in touch.

Nevertheless, in the absence of any shell corection it is not possible to reproduce the experimental data, or to give results for particle-accompanied fission. By adding (phenomenological) shell corrections we succeded to obtain minima at a finite value of mass asymmetry for the binary fission of $^{226-238}$Th and $^{230-238}$U nuclei.

Fission barriers for ternary and quaternary fission into identical fragments are lower than for aligned spherical fragments in touch. Our expectations concerning the possibilty to detect quaternary fission as 2α-accompanied fission were experimentally confirmed.

Acknowledgements

This work was partly supported by the Frankfurt Institute for Advanced Studies, by a grant of the Deutsche Forschungsgemeinschaft, and by Ministry of Education and Research, Bucharest.

References

[1] D. N. Poenaru and W. Greiner, in *Nuclear Decay Modes*, Institute of Physics, Bristol, 1996, Chap. 6, p. 275.

[2] D. N. Poenaru, Y. Nagame, R. A. Gherghescu, and W. Greiner, *Phys. Rev.* **C 65** (2002) 054308; Erratum: **C 66** (2002) 049902.

[3] G. Royer and R. Moustabchir, *Nucl. Phys.* **A 683** (2001) 182.

[4] M. Mutterer and J. P. Theobald, Chap. 12 in [1] p. 487.

[5] J. H. Hamilton *et al J. Phys. G* **20** (1994) L85.

[6] J. H. Hamilton *et al.*, *Prog. Part. Nucl. Phys.* **35** (1995) 635.

[7] A. V. Ramayya *et al.*, *Phys. Rev. Lett.* **81** (1998) 947; *Phys. Rev. C* **57** (1998) 2370.

[8] D. N. Poenaru, B. Dobrescu, W. Greiner, J. H. Hamilton, and A. V. Ramayya, *J. Phys. G* **26** (2000) L97.

[9] D. N. Poenaru, W. Greiner, J. H. Hamilton, A. V. Ramayya, E. Hourany and R. A. Gherghescu, *Phys. Rev., C* **59** (1999) 3457.

[10] F. Gönnenwein, P. Jesinger, M. Mutterer, A. M. Gagarski, G. Petrov, W. H. Trzaska, V. Nesvizhevski, O. Zimmer, in *Nuclear Physics at Border Lines (Proc. Internat. Conf. Lipari, 2001)* (World Scientific, Singapore, 2002), Eds. G. Fazio et al. p. 107.

[11] F. Gönnenwein, P. Jesinger, M. Mutterer, W. H. Trzaska, G. Petrov, A. M. Gagarski, V. Nesvizhevski, P. Geltenbort, *Heavy Ion Physics* **18** (2003) 419.

[12] A. Gavron, *Phys. Rev. C* **11** (1975) 580.

[13] Y. Nagame *et al.*, *Phys. Lett. B* **387** (1996) 26; *Radiochimica Acta* **78** (1997) 3; *J. Radioanal. Nucl. Chem.* **239** (1999) 97.

[14] I. Nishinaka *et al.*, *Phys. Rev., C* **56** (1997) 891.

[15] T. Ohtsuki, Y. Nagame, and H. Nakahara, in *Heavy Elements and Related New Phenomena*, World Sci., Singapore, 1999, Vol. I, Chap. 13, p. 507.

[16] Y. L. Zhao *et al.*, *Phys. Rev. Lett.* **82** (1999) 3408; *Phys. Rev. C* **62** (2000) 014612.

[17] S. Cohen and W. J. Swiatecki, *Ann. Physics (N. Y.)* **22** (1963) 406.

[18] V. M. Strutinsky, *JETF* **42** (1962) 1571.

[19] R. W. Hasse and W. D. Myers, *Geometrical relationships of macroscopic nuclear physics* (Springer, Berlin, 1988).

[20] R. Smolańczuk, H. V. Klapdor-Kleingrothaus and A. Sobiczewski, *Acta Physica Polonica, B* **24** (1993) 685.

[21] P. Möller, D. G. Madland, A. J. Sierk and A. Iwamoto, *Nature* **409** (2001) 785.

[22] V. M. Strutinsky, *Nucl. Phys.* **A 96** (1967) 420.

[23] D. N. Poenaru, W. Greiner, Y. Nagame, and R. A. Gherghescu, *J. Nucl. Radiochem. Sci., Japan*, **3** (2002) 43.

[24] D. N. Poenaru and W. Greiner, *Europhysics Letters* **64** (2003) 164.

[25] G. B. Arfken and H. J. Weber, *Mathematical methods for physicists* (Academic Press, London, 1995).

[26] E. W. Weisstein, From MathWorld — A Wolfram Web Resource http://mathworld.wolfram.com/MeanCurvature.html

[27] H. Lamb, *Hydrodinamics* (Cambridge University Press, New York, 1932).

[28] L. D. Landau and E. M. Lifshitz, *Fluid Mechanics* (Pergamon, London, 1959).

[29] D. N. Poenaru et al., *Z. Phys.* **A 333** (1989) 291.

[30] D. N. Poenaru and M. Ivaşcu, *Comp. Phys. Communic.* **16** (1978) 85.

[31] D. N. Poenaru, M. Ivaşcu, and D. Mazilu, *Comp. Phys. Communic.* **19** (1980) 205.

[32] W. D. Myers and W. J. Swiatecki, *Nucl. Phys. A* **81** (1966) 1.

[33] H. Schultheis and R. Schultheis, *Phys. Lett. B* **37** (1971) 467.

[34] H. R. von Gunten, Actinides Rev. **1**, 275 (1969).

[35] E. A. C. Croach, Atomic Data Nucl. Data Tables **19**, 417 (1977).

[36] Wilkins, P. D., Steinberg, E. P. and Chasman, R. R. *Phys. Rev.* **C 14** (1976) 1832.

[37] A. C. Wahl, *Atomic Data Nucl. Data Tables* **68** (1998) 91.

[38] R. A. Gherghescu, *Phys. Rev.* **C 67** (2003) 014309.

[39] D. N. Poenaru, W. Greiner, and R. A. Gherghescu, *Atomic Data Nucl. Data Tab.* **68** (1998) 91.

[40] H. Diehl and W. Greiner, *Nucl. Phys. A* **229** (1974) 29.

[41] R. D. Present, *Phys. Rev.* **59** (1941) 466.

[42] L. Rosen and A. M. Hudson, *Phys. Rev.* **78** (1950) 533.

[43] R. H. Iyer and J. W. Cobble, *Phys. Rev.* **172** (1968) 1186.

[44] P. Schall, P. Heeg, M. Mutterer, and J. P. Theobald, *Phys. Lett. B* **191** (1987) 339.

[45] R. L. Fleischer, P. B. Price, R. M. Walker, and E. L. Hubbard, *Phys. Rev.* **143** (1966) 943.

[46] D. L. Hill, in Proc. 2nd U. N. Int. Conf. on the *Peaceful Uses of Atomic Energy*, Geneva, 1-13 Sept, 1958, United Nations, Geneva, 1958 p. 244.

[47] W. J. Swiatecki, in Proc. 2nd U. N. Int. Conf. on the *Peaceful Uses of Atomic Energy*, Geneva, 1-13 Sept, 1958, United Nations, Geneva, 1958 p. 248.

[48] D. N. Poenaru and W. Greiner, *J. Phys. G: Nucl. Part. Phys.* **25** (1999) L7.

[49] D. N. Poenaru, W. Greiner, J.H. Hamilton, E. Hourany, R. A. Gherghescu, in *Perspectives in Nuclear Physics* Eds. J. H. Hamilton, H. K. Carter, R. B. Piercey (World Scientific, Singapore, 1999) p. 307.

[50] D. N. Poenaru, W. Greiner, J. H. Hamilton, and A. V. Ramayya, *J. Phys. G* **27** (2001) L19.

[51] W. Scheid and W. Greiner, *Z. Phys.* **A226** (1969) 364.

[52] H. J. Krappe, J. R. Nix and A. J. Sierk, *Phys. Rev.* **C20** (1979) 992.

APPENDIX: Euler - Lagrange equation

The functional to be minimized is the surface and Coulomb energy (given in equation (3)) with the constraints (eqs. 4, 5). We denote with F_1, F_2, F_3, F_4, the corresponding integrands one needs to write the Euler-Lagrange equation:

$$\sigma F_1 = \sigma\rho\left(1+\rho'^2\right)^{1/2} \tag{42}$$

$$\frac{R_0\rho_e\phi_s}{5}F_2 = \frac{R_0\rho_e\phi_s}{5}\left(\rho^2 - z\rho\rho'\right) \tag{43}$$

$$F_3 = \rho^2 \tag{44}$$

$$F_4 = \rho^2 F \tag{45}$$

The derivatives are easily obtained

$$\frac{\partial F_1}{\partial\rho} = \left(1+\rho'^2\right)^{1/2} \tag{46}$$

$$\frac{d}{dz}\frac{\partial F_1}{\partial\rho'} = \frac{d}{dz}\left[\frac{\rho\rho'}{(1+\rho'^2)^{1/2}}\right] = \frac{\rho'^2+\rho\rho''}{(1+\rho'^2)^{1/2}} - \frac{\rho\rho'^2\rho''}{(1+\rho'^2)^{3/2}} \tag{47}$$

$$\frac{\partial F_2}{\partial \rho} = 2\rho - z\rho' \tag{48}$$

$$\frac{d}{dz}\frac{\partial F_2}{\partial \rho'} = \frac{d}{dz}(-z\rho) = -\rho - z\rho' \tag{49}$$

$$\frac{\partial F_3}{\partial \rho} = 2\rho \tag{50}$$

$$\frac{\partial F_4}{\partial \rho} = 2\rho\left(F + \frac{\rho}{2}\frac{\partial F}{\partial \rho}\right) \tag{51}$$

Consequently the Euler-Lagrange equation can be written as

$$\sigma\left(\frac{\partial F_1}{\partial \rho} - \frac{d}{dz}\frac{\partial F_1}{\partial \rho'}\right) + \frac{R_0\rho_e\phi_s}{5}\left(\frac{\partial F_2}{\partial \rho} - \frac{d}{dz}\frac{\partial F_2}{\partial \rho'}\right) + \rho\left(2\lambda_1'' + 2\lambda_2'' f\right) = 0 \tag{52}$$

leading to

$$\rho\rho'' - \rho'^2 - (\lambda_1 + \lambda_2|z| + 6XV_s)\,\rho(1+\rho'^2)^{3/2} - 1 = 0 \tag{53}$$

if we choose $F = |z|$ (hence $f = |z|$) and express $3R_0\rho_e/(5\sigma)$ as $6X$ because the Coulomb and surface energy of a spherical nucleus within LDM are given by $E_C^0 = (3Z^2e^2)/(5R_0)$ and $E_s^0 = 4\pi R_0^2\sigma$, respectively.

Alternatively one can obtain from this equation the equivalent relationship

$$2\sigma K + 3\rho_e\phi_s/5 + \lambda_1' + \lambda_2' f = 0 \;\;;\;\; f(z,\rho) = F(z,\rho) + \frac{\rho}{2}\frac{\partial F(z,\rho)}{\partial \rho} \tag{54}$$

in which the definition of the mean curvature, K, from section 3 was used.

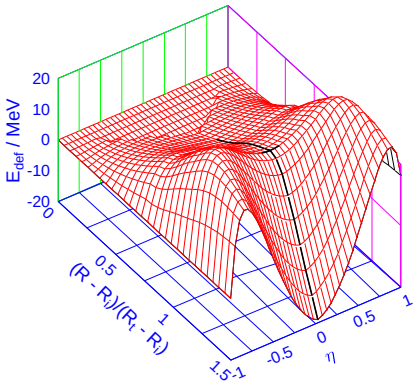

Figure 1: An example of a potential energy surface $E_{def} = E_{def}(R, \eta)$ calculated within liquid drop model, with a statical path marked with the heavy line which has a cross at the saddle point.

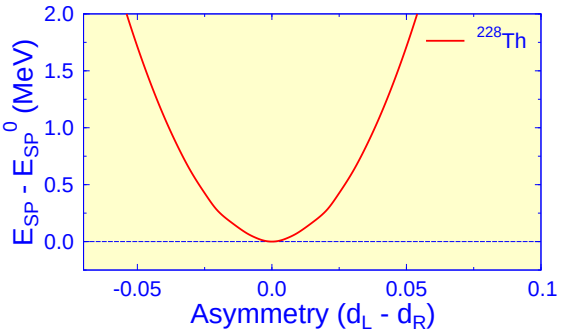

Figure 2: The saddle point deformation energy E_{SP} vs. mass-asymmetry within a pure liquid drop model. Example of ^{228}Th.

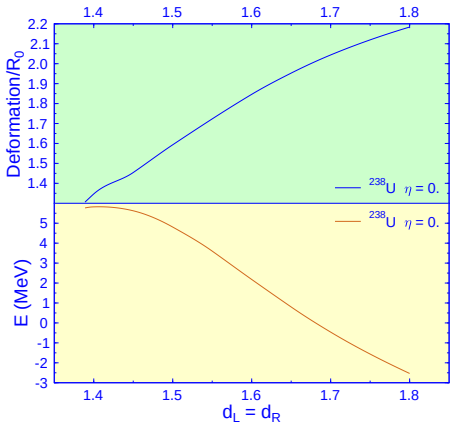

Figure 3: Deformation and potential energy vs. input parameter of the integro-differential equation for binary fission of ^{238}U within a pure LDM.

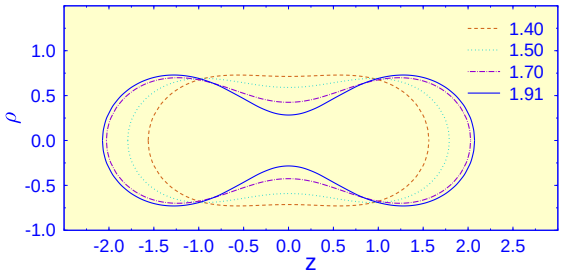

Figure 4: Nuclear shapes during binary fission of a nucleus with fissility $X = 0.60$ for $d_L = d_R = 1.40, 1.50, 1.70, 1.91$.

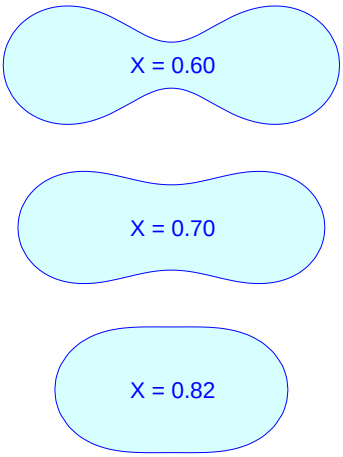

Figure 5: Sadle-point shapes during binary fission of nuclei with fissility $X = 0.60, 0.70, 0.82$.

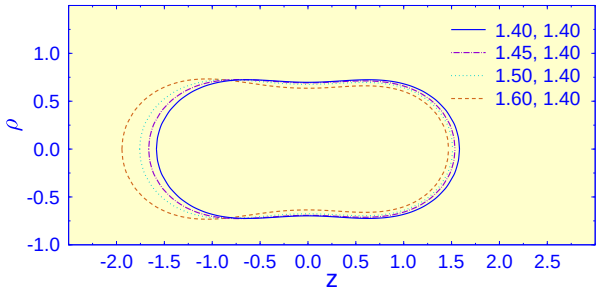

Figure 6: Mass asymmetric shapes during binary fission of a nucleus with fissility $X = 0.60$ for $d_L \neq d_R$. Pure LDM calculations.

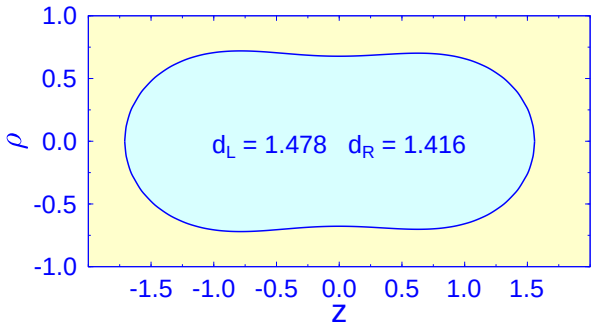

Figure 7: Mass asymmetric saddle point shape of ^{232}U. Shell effects taken into account.

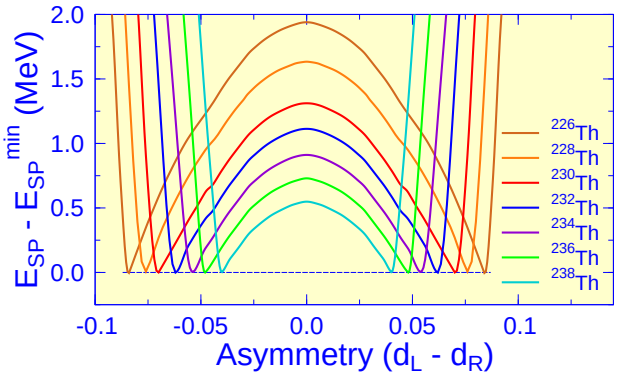

Figure 8: Difference between the saddle point deformation energy E_{SP} and its minimum value E_{SP}^{min} vs mass asymmetry parameter [related to $(d_L - d_R)$] for binary fission of Th isotopes. One can see the minima produced by the shell effects.

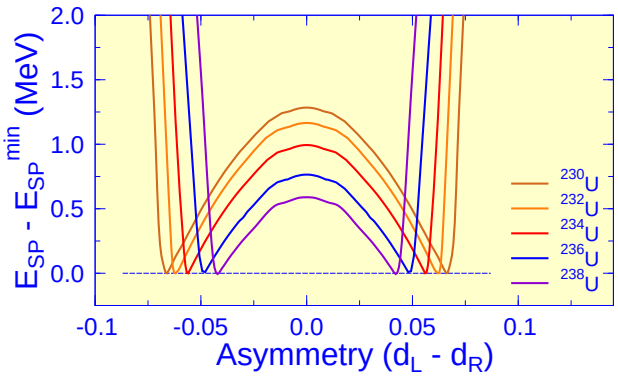

Figure 9: Difference between the saddle point deformation energy E_{SP} and its minimum value E_{SP}^{min} vs mass asymmetry parameter [related to $(d_L - d_R)$] for binary fission of U isotopes in the presence of shell corrections.

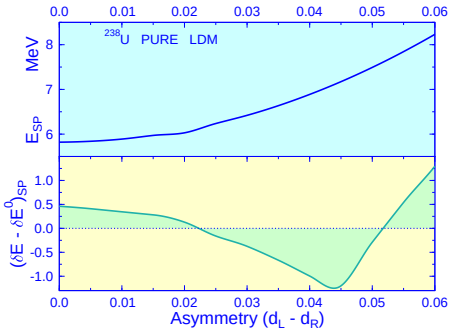

Figure 10: The saddle point deformation energy E_{SP} of ^{238}U within a pure liquid drop model (top). The minimum of the E_{SP} is produced by the negative values of the shell corrections $(\delta E - \delta E^0)_{SP}$ (bottom).

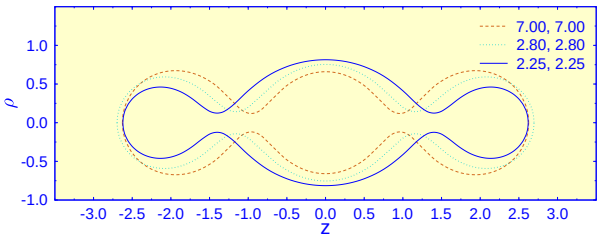

Figure 11: Shapes obtained by solving an integro-differential equation for $n_L = n_R = 3$, $d_L = d_R = 2.25, 2.80$, and 7.00. The binary fissility $X = 0.60$ corresponds to ^{170}Yb.

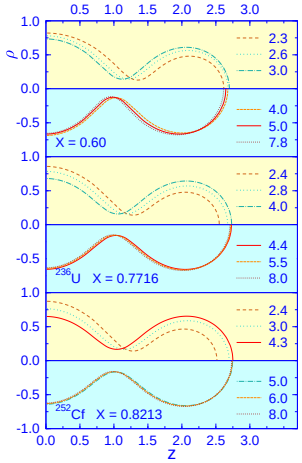

Figure 12: Evolution of ternary shapes ($n_L = n_R = 3$) when the input paramter $d_L = d_R$ is increased as shown for ^{170}Yb (top), ^{236}U (middle), and ^{252}Cf (bottom). The total length on the symmetry axis increases with increasing $d_L = d_R$ in the upper part of the panel and decreases in the lower part.

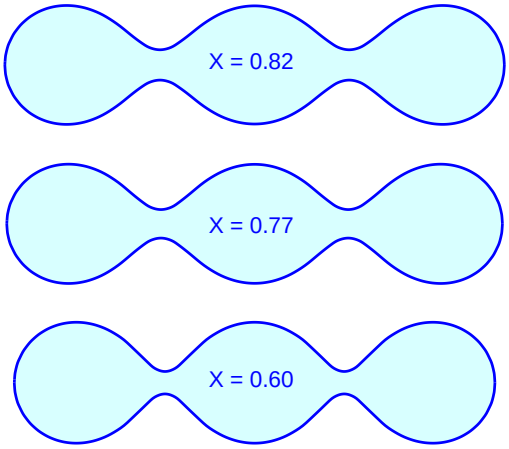

Figure 13: Ternary shapes ($n_L = n_R = 3$) approaching a scission into three fragments with identical radii ^{170}Yb (bottom), ^{236}U (middle), and ^{252}Cf (top).

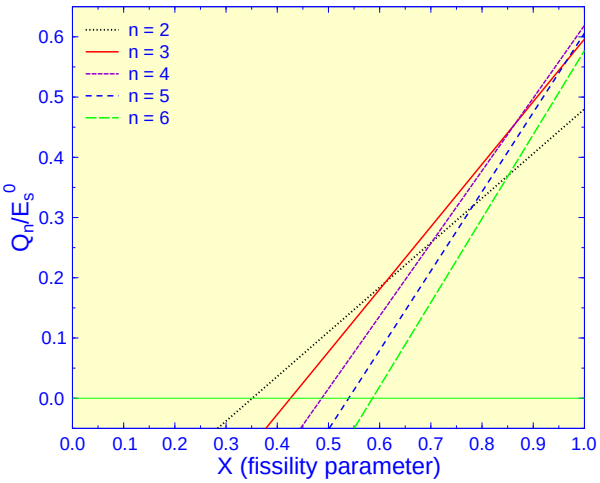

Figure 14: Approximation of Q-values for fission into equally sized fagments.

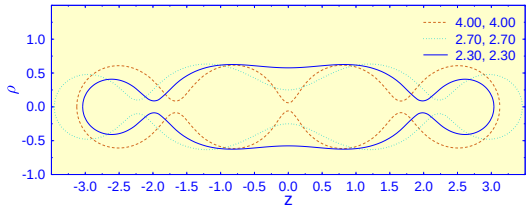

Figure 15: Nuclear shapes during quaternary fission of a nucleus with fissility $X = 0.60$ for $d_L = d_R = 2.30, 2.70, 4.00$.

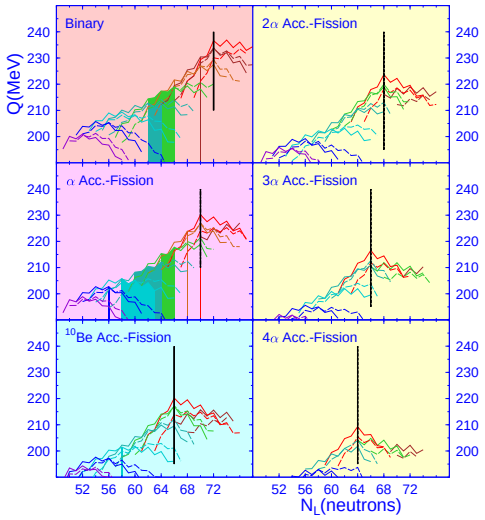

Figure 16: Q-values for the cold fission of ^{252}Cf vs. neutron number of the light fragment. The experimentally determined cold fission, α-, and ^{10}Be accompanied fission on the left hand side are emphasized. The vertical heavy bar on each graph corresponds to a magic neutron number of the heavy fragment $N_H = 82$.

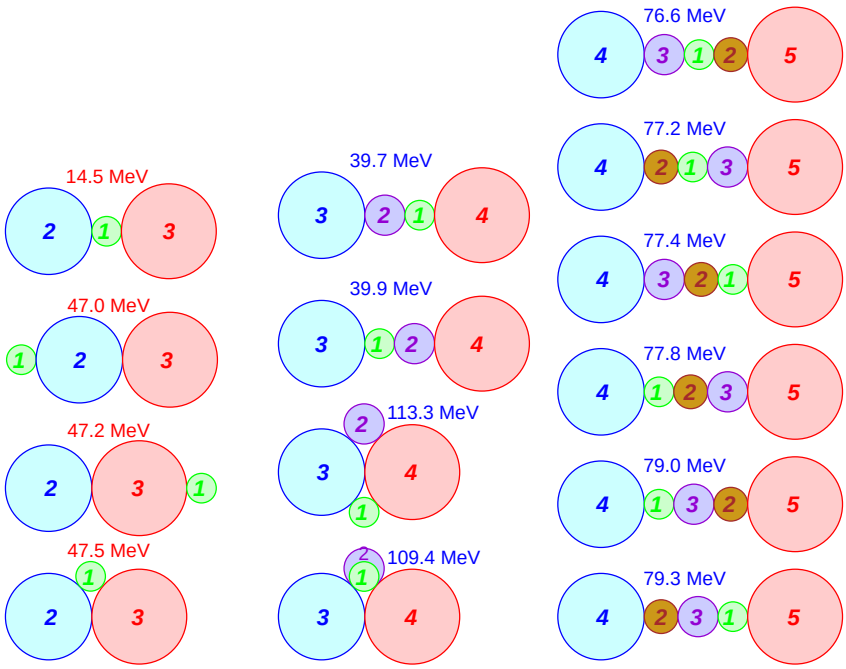

Figure 17: Aligned and compact configurations for α accompanied cold fission (left hand side) and for α + ^{10}Be accompanied cold fission (middle). On the right hand side there are aligned configurations with three clusters between the light and heavy fragment for α + ^{6}He + ^{10}Be accompanied cold fission. The parent is ^{252}Cf, and the heavy fragment is the doubly magic ^{132}Sn. The corresponding energies are shown.

Table 1: Conditional saddle point elongation parameter d_{R-SP} and energy E_{SP} for a given asymmetry $d_L - d_R$ within a pure liquid drop model for ^{238}U parent nucleus.

d_{R-SP}	$d_L - d_R$	E_{SP} (MeV)
1.405	0.000	5.822
1.400	0.005	5.840
1.400	0.010	5.889
1.395	0.015	5.972
1.410	0.020	6.029
1.395	0.025	6.237
1.390	0.030	6.420
1.390	0.035	6.637
1.390	0.040	6.888
1.390	0.045	7.172
1.390	0.050	7.492
1.390	0.060	8.232
1.390	0.070	9.115
1.395	0.080	10.144

Table 2: Conditional saddle point elongation parameter d_R and energy E_{SP} for a given asymmetry $d_L - d_R$ within liquid drop model plus phenomenological shell correction for ^{238}U parent nucleus. The shell correction for the spherical parent $\delta E^0 = -5.385$ MeV. For $d_L - d_R < 0.045$ the d_R at which E_{SP} is maximum differs from d_R at which its LDM part is maximum.

d_R	$d_L - d_R$	E_{SP-LDM} MeV	$\delta E_{SP} - \delta E^0$ MeV	E_{SP} MeV
1.385	0.000	5.728	0.462	6.189
1.390	0.000	5.775	0.413	6.188
1.385	0.005	5.769	0.410	6.179
1.410	0.005	5.823	0.286	6.109
1.395	0.010	5.804	0.345	6.150
1.405	0.010	5.859	0.250	6.109
1.385	0.015	5.936	0.146	6.082
1.390	0.015	5.841	0.282	6.123
1.385	0.020	6.062	-0.064	5.998
1.390	0.020	5.953	0.129	6.082
1.385	0.025	6.219	-0.327	5.892
1.400	0.025	6.108	-0.161	5.948
1.385	0.030	6.408	-0.642	5.766
1.395	0.030	6.233	-0.375	5.858
1.385	0.035	6.628	-1.010	5.618
1.395	0.035	6.421	-0.665	5.755
1.385	0.040	6.881	-1.431	5.450
1.395	0.040	6.634	-0.996	5.639
1.415	0.045	7.044	-1.201	5.844
1.405	0.050	7.445	-0.289	7.155
1.400	0.055	7.825	0.541	8.366
1.395	0.060	8.229	1.296	9.525
1.390	0.065	8.657	2.403	11.059